JOURNAL OF GEOPHYSICAL RESEARCH, VOL. 99, NO. C8, PAGES 16,001–16,017, AUGUST 15, 1994

Heat and salt balances over the northern California shelf in winter and spring

E. P. Dever and S. J. Lentz

Department of Physical Oceanography, Woods Hole Oceanographic Institution, Woods Hole, Massachusetts

Abstract. Heat and salt balances are estimated over the northern California shelf from early December 1988 through late February 1989 (winter) and from early March through early May 1989 (spring) from moored meteorological and oceanographic time series taken in 93 m of water 6.3 km from the coast. We find a winter mean offshore heat flux of 8.7×10^5 W m^{-1}, about a factor of 5 smaller than earlier estimates of the mean summer (upwelling season) offshore heat flux on the northern California shelf. The mean offshore heat flux is predominantly in the surface boundary layer and is balanced by an along-shelf heat flux divergence (as represented by an eddy along-shelf temperature gradient flux) and a cooling trend making the mean winter heat balance fundamentally three dimensional. In contrast to winter, the spring mean offshore heat flux of 6.4×10^5 W m^{-1} is balanced by a positive air-sea heat flux of 8.3×10^5 W m^{-1}, which is about 80% of the mean air-sea heat flux in summer. This makes the spring mean heat budget primarily two dimensional, like the summer mean heat budget off northern California. On timescales of days the dominant terms in the fluctuating heat budget in both winter and spring are the cross-shelf heat flux and local changes in heat content. These are well correlated with each other and with the local along-shelf wind stress. The along-shelf temperature gradient flux, uncorrelated with the along-shelf wind stress, is usually weak on timescales of days. Occurrences when it is strong are interpreted as effects of mesoscale features. Mean and fluctuating cross-shelf salt fluxes provide essentially the same information as cross-shelf heat fluxes. This is not surprising in light of the strong temperature-salinity relationship on the northern California shelf.

1. Introduction

The coast of northern California exhibits two distinct seasons, a summer upwelling season and a winter–spring storm season [*Strub et al.*, 1987a; *Lentz and Chapman*, 1989]. These seasons are typically separated by a rapid spring transition [*Lentz*, 1987a] and a more gradual fall transition [*Strub and James*, 1988]. Mean meteorological conditions during the summer upwelling season are distinguished by strong positive (from the atmosphere to the ocean) sea surface heat flux [*Nelson and Husby*, 1983; *Lentz*, 1987b] and strong persistent equatorward winds [*Nelson*, 1977; *Strub et al.*, 1987b]. In response to the equatorward wind stress and a negative along-shelf pressure gradient [*Hickey and Pola*, 1983], along-shelf mean currents are equatorward near the surface and exhibit vertical shear, becoming weaker and sometimes poleward near the bottom, and mean cross-shelf currents are offshore near the surface and near zero in the interior [*Winant et al.*, 1987].

Studies of the summer heat budget over the northern California shelf show that the equatorward wind stress and resulting circulation produce a large mean offshore flux of heat in the surface boundary layer [*Lentz*, 1987b; *Rudnick and Davis*, 1988; *Send*, 1989] characteristic of coastal upwelling. The magnitude of the mean cross-shelf heat flux is similar to that found during upwelling conditions in other regions such as Oregon and northwest Africa [*Bryden et al.*, 1980; *Richman and Badan-Dangon*, 1983] and, as in these other upwelling regions, a positive mean sea surface heat flux balances the mean offshore heat flux. Off northern California, alongshore heat transport and in situ cooling play secondary roles in the mean heat balance for summer, and the role of onshore eddy heat flux is still unclear. In a volume heat budget, *Lentz* [1987b] finds only a small contribution due to cross-shelf eddy heat flux. In a study considering a single mooring at midshelf, *Send* [1989] finds a much stronger onshore eddy heat flux which he attributes to wind forcing.

Though there have been several studies of the heat budget for the upwelling season in coastal regions, there have been few studies of the heat budget under nonupwelling conditions which exist over the northern California shelf during the winter and early spring months. From December until the spring transition in April or May, monthly mean along-shelf wind stresses on the northern California shelf are typically weak and may be poleward [*Nelson*, 1977]. And from December to February, monthly mean surface heat fluxes are weak or even negative, becoming persistently positive and stronger in March [*Nelson and Husby*, 1983]. Mean along-shelf currents are poleward and less vertically sheared than in summer, and mean cross-shelf currents are much weaker [*Lentz and Chapman*, 1989]. All this suggests the heat budget on the northern California shelf during winter and spring may be quite different from that during the summer upwelling season.

Paper number 94JC01228.
0148-0227/94/94JC-01228$05.00

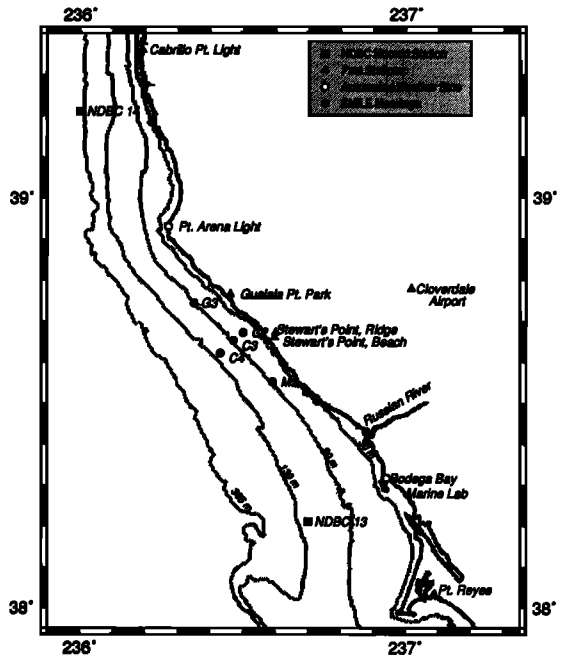

Figure 1. Map of SMILE region. The central mooring location was chosen to be near the CODE C3 mooring location. This study will primarily use data from the central C3 mooring and the along-shelf G3 and M3 moorings.

The mean and fluctuating heat and salt balances during winter and spring are studied using data collected at a midshelf mooring site off northern California from December 1988 to May 1989. We introduce these data in section 2. In section 3 we develop the heat (and salt) balance equations per unit along-shelf distance and the methods used to estimate the terms in these balances from the data. The heat and salt balances are presented in section 4. We compare our results to previous studies of summer upwelling heat balances and discuss their general applicability in light of climatological data in section 5.

2. Observations

2.1. Field Program

This study uses observations from the Shelf Mixed Layer Experiment (SMILE) and the Sediment Transport Events over the Shelf and Slope (STRESS) studies. These field programs took place over the northern California shelf from mid-November 1988 to mid-May 1989 in the same region as the previous Coastal Ocean Dynamics Experiment (CODE) [*Beardsley and Lentz*, 1987]. The central element of the SMILE array was a surface mooring, denoted C3, located at 38°38.71'N, 123°129.56'W in 93 m of water (Figures 1 and 2). C3 was deployed November 12, 1988, and recovered May 19, 1989. This mooring supported vector-measuring current meters (VMCMs) with temperature sensors at 12 depths from 5.5 to 49.5 m (Figure 2) and a surface meteorological package. Conductivity was measured with SeaBird SeaCats at six depths (VMCM/C) from 8.5 m to 49.5 m. A STRESS subsurface mooring, within 0.5 km of the SMILE surface mooring and also denoted C3, was deployed December 6, 1988, recovered February 27, 1989, and turned around and redeployed from March 3 to May 5, 1989, by B. Butman, U.S. Geological Survey (USGS). The STRESS mooring had five vector-averaging current meters (VACMs) with temperature sensors between 30 and 6 m above the bottom (Figure 2). Three VACMs were also equipped with SeaBird conductivity cells (VACM/C). Together, the C3 SMILE and STRESS moorings provided excellent vertical resolution in temperature from 5.5 m below the surface to 6 m above the bottom. Though current observations initially had the same resolution, several VMCMs developed bearing corrosion problems which caused them to fail before the end of the 6-month deployment, and one VACM did not provide usable velocity data during its second deployment (Figure 3).

In addition to the central SMILE and STRESS C3 moorings, some use will be made of the peripheral SMILE moorings (Figure 1). The G3 and M3 moorings, approximately 15 km north and south of C3 and with similar temperature resolution, will be used to characterize along-shelf temperature gradients in the upper 49.5 m. They resembled the C4 mooring shown in Figure 2. VMCM current data exist at 10 m; however, upward looking acoustic Doppler current profilers (ADCPs) at G3 and M3 failed shortly after deployment. Also, temperature observations at C2 (not present in winter) will be used to check estimates of heat content change in spring. Further information concerning the mooring locations, deployment times, configurations, and data return from the SMILE and STRESS experiments are given by *Alessi et al.* [1991].

For reasons related to data coverage (Figure 3) and the local air-sea heat flux (Figure 4), the data were divided into

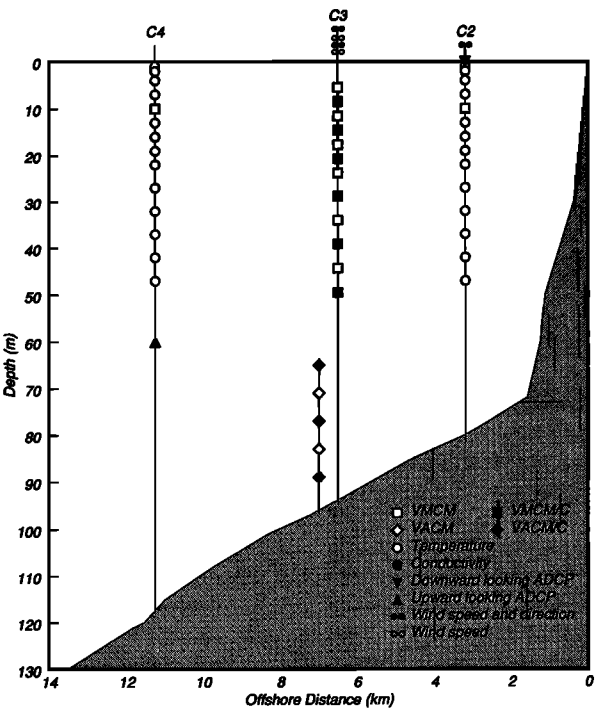

Figure 2. Cross section of shelf showing moorings and instrument locations. The central C3 site includes a surface mooring with instruments spanning the upper 49.5 m and a subsurface mooring with instruments spanning the lower 30 m deployed as part of STRESS. Along-shelf moorings at G3 and M3 (Figure 1) had configurations similar to the C4 mooring.

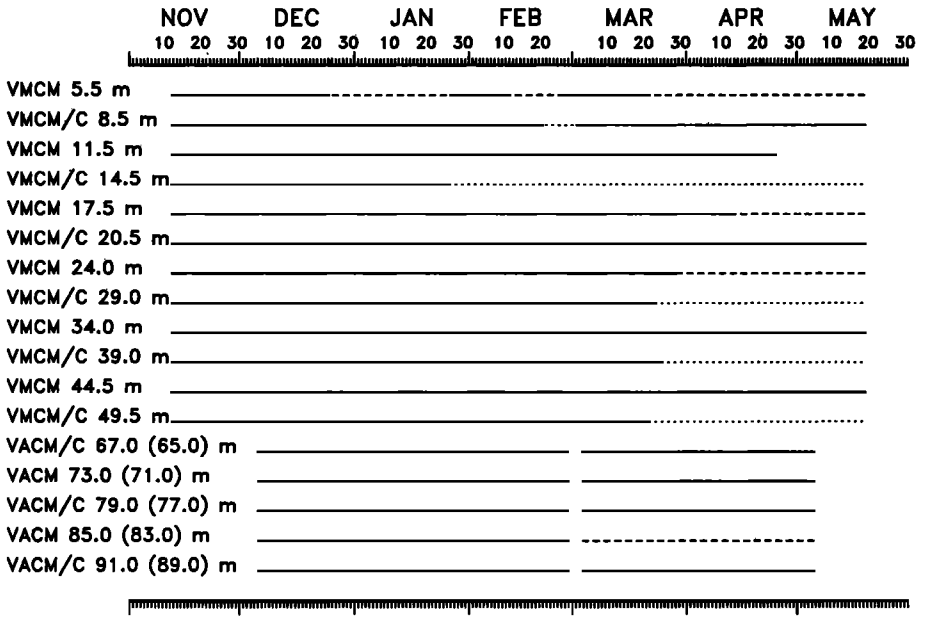

Figure 3. Data return for the SMILE and STRESS C3 moorings. Though many VMCM (and one VACM) velocity sensors (solid lines) failed early, almost all temperature (long-dashed lines) and temperature and conductivity sensors (short-dashed lines) returned complete records.

two time periods: 0400 UT on December 6, 1988, to 2300 UT on February 20, 1989 (winter), and 2200 UT on March 3 to 0400 UT on May 2, 1989 (spring). The names winter and spring were chosen not on the basis of large-scale meteorological patterns, such as the positions and strengths of the North Pacific subtropical high and Aleutian low (C. E. Dorman et al., Structure of the lower atmosphere over the northern California coast during winter, submitted to *Monthly Weather Review*, 1994, hereinafter referred to as C. E. Dorman et al., submitted manuscript, 1994) [*Halliwell and Allen*, 1987; *Strub et al.*, 1987b; *Lentz*, 1987a], but rather the effect of local air-sea heat flux on the mean heat budget. The winter period covers the meteorological conditions which contrast most strongly from summer upwelling conditions in that mean winds and sea surface heat flux (Figure 4) are both weak. During spring, mean winds were again weak but surface heating increased, distinguishing this time period from winter. Though current meter failures began to

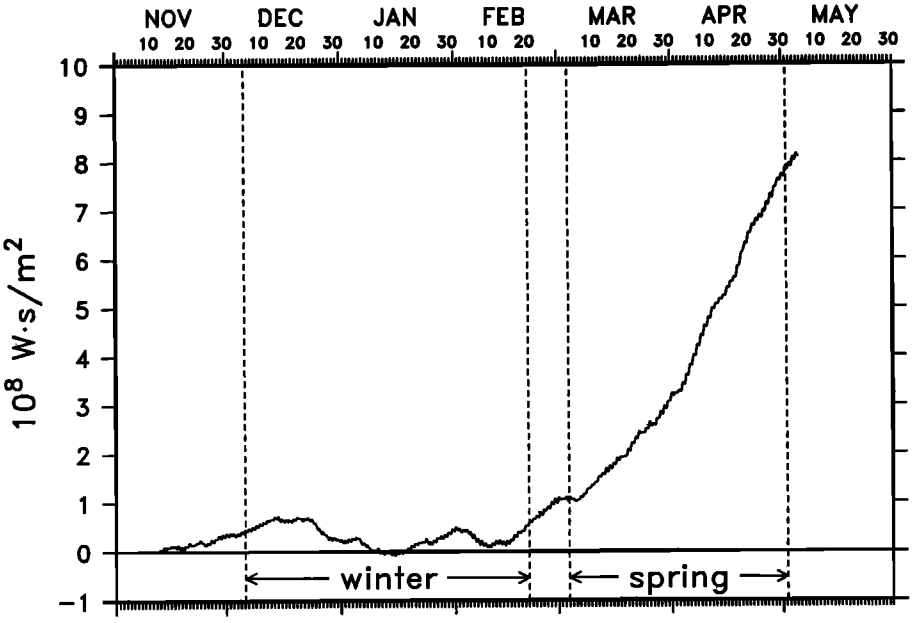

Figure 4. Total energy added/subtracted by net air-sea heat flux from November 1988 to May 1989. From November until the beginning of March the surface heat flux is small, variable, and often from the ocean to the atmosphere. Beginning in March the surface heat flux becomes persistently positive. A change of 10^8 W s m^{-2} corresponds to a change in the depth-averaged temperature at C3 (93 m depth) of 0.26°C.

affect severely near-surface velocity resolution during spring, we believe this does not change the qualitative results.

2.2. Mean Winter and Spring Conditions

Before estimating the heat budgets in winter and spring, mean observations from these time periods are presented to give an overview and comparison to historical CODE data taken during the summers of 1981 and 1982 and the intervening winter. Velocity data are presented in a reference frame approximately parallel to local isobaths at C3 and identical to that of the CODE program [*Winant et al.*, 1987]. In this coordinate system the along-shelf direction y is defined such that $y = 0$ at C3 and increases toward 317°T. The cross-shelf direction x is defined such that $x = 0$ at the coast and decreases offshore. Cross-shelf and along-shelf velocities are denoted u and v, respectively. The mean cross-shelf transport in this coordinate frame was nearly zero during both winter and spring. Rotations of 3.7° clockwise in winter and less than 0.3° counterclockwise in spring gave zero mean cross-shelf transport. These rotations did not qualitatively affect any of the results discussed in this paper; therefore only results in the 317° reference frame will be presented.

In winter during both SMILE and CODE, mean along-shelf wind stress was weak (0.03 N m^{-2} in both years) and equatorward. Though upwelling favorable, it was a factor of 4–6 less than the wind stress averaged over similar record lengths during summer [*Winant et al.*, 1987]. The mean SMILE sea surface heat flux in winter was 2 W m^{-2} as compared to climatological monthly mean values of nearly 200 W m^{-2} in June, July, and August [*Nelson and Husby*, 1983]. Figure 5 shows mean observations from the winter 1988–1989 (SMILE) and from a similar period during winter 1981–1982 CODE [*Lentz and Chapman*, 1989]. Mean winter cross-shelf currents were similar for CODE and SMILE, 1–3 cm s^{-1} offshore in the upper 30 m, onshore in the interior with a maximum of about 2 cm s^{-1}, and offshore from 75 m to near bottom during SMILE (Figure 5a). In contrast during the summers of 1981 (CODE 1) and 1982 (CODE 2), mean offshore currents at C3 (not shown) exceeded 6 cm s^{-1} in the upper 30 m, and mean cross-shelf currents were weak (~1 cm s^{-1}) below 30 m [*Winant et al.*, 1987]. During SMILE, winter mean along-shelf currents were poleward with a maximum speed of over 6 cm s^{-1} from about 50 to 75 m and weaker flow near the surface and bottom. During CODE, winter mean along-shelf currents were poleward with speeds of about 5 cm s^{-1} but were not as vertically sheared. By contrast, summer 1982 [*Winant et al.*, 1987] mean along-shelf currents were equatorward and vertically sheared with speeds of over 7 cm s^{-1} near the surface and weaker flow below 40 m at C3. Mean vertical temperature and salinity gradients were 0.01°C m^{-1} and 0.005 practical salinity units (psu) m^{-1}, respectively, for winter 1988–1989 (see Figures 5c and 5d). These gradients are comparable to, but slightly smaller than, the mean temperature and salinity gradients reported for summer by *Winant et al.* [1987] and *Huyer* [1984].

In spring the equatorward mean along-shelf wind stress was less than 0.02 N m^{-1}, and the mean sea surface heat flux during this time period was 133 W m^{-2}, approaching typical summer values. Mean near-surface cross-shelf currents were even weaker than in winter and were offshore only at 8.5 m

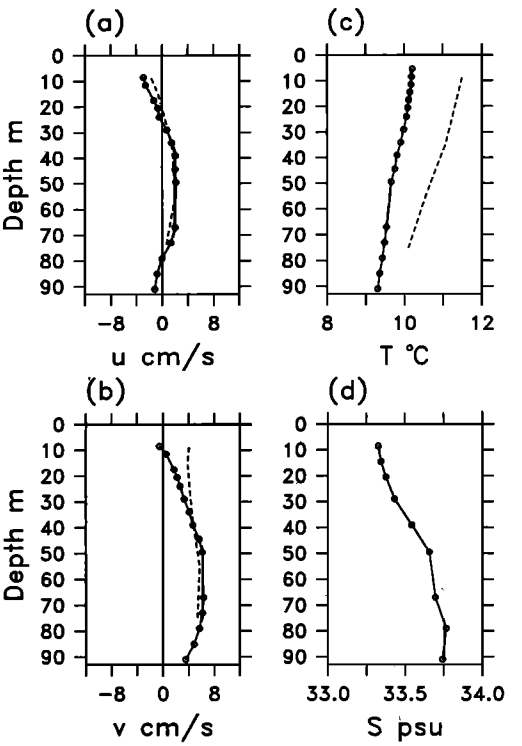

Figure 5. Mean winter (a) cross-shelf and (b) along-shelf velocity profiles at C3. The solid line indicates means between 0400 UT on December 6, 1988, and 2300 UT on February 20, 1989 (SMILE), and the dashed line indicates means between 1300 UT on December 12, 1981, and 1200 UT on March 22, 1982 (CODE). Mean (c) temperature and (d) salinity profiles are also shown. No salinity time series were collected during the 1981–1982 time period. Means are only shown for records lasting the entire time period. For SMILE/STRESS these depths are indicated by circles.

(Figure 6a). Mean along-shelf currents (Figure 6b) were more vertically sheared than in winter. Near the surface, flow was equatorward with a speed over 11 cm s^{-1}. It became weaker with depth and was poleward below 70 m. While this sheared equatorward flow is similar to the mean flow in summer, the weak equatorward mean wind stress and high temperature and low salinity at C3 suggest it was caused by a mesoscale feature over the outer shelf and slope in March and April 1989 (see also *Largier et al.* [1993]), not by wind-driven upwelling. Spring mean temperature and salinity profiles (Figures 6c and 6d) were bilinear in character. Above 49.5 m, vertical gradients were 0.04°C m^{-1} in temperature and 0.013 psu m^{-1} in salinity. These gradients were about 3 times those observed in winter and about twice those observed in upwelling season [*Winant et al.*, 1987]. Below 49.5 m, mean vertical gradients were 0.01°C m^{-1} and 0.005 psu m^{-1}, similar to those observed in winter.

3. Methods

3.1. Developing the Heat Budget Equations

Surface to bottom vertical coverage existed only at the central C3 mooring. This constrained us to look at the heat budget over a two-dimensional cross-shelf area bounded vertically by the bottom, $z = -H(x)$, and the surface, $z =$

0, and in the cross-shelf direction by the C3 mooring, $x = -L$, and the coast, $x = 0$. The heat budget for this area is

$$\rho c_p \int_{-L}^{0} dx \int_{-H}^{0} \frac{\partial T}{\partial t}\, dz = \rho c_p \left[\int_{-H}^{0} uT|_{x=-L}\, dz - \int_{-L}^{0} dx \int_{-H}^{0} \left(T \frac{\partial v}{\partial y} + v \frac{\partial T}{\partial y} \right) dz \right] + \int_{-L}^{0} Q\, dx \qquad (1)$$

where ρc_p is the heat capacity per unit volume (assumed constant and equal to 4.1×10^6 W s m^{-3} °C^{-1}), T is the water temperature, and Q is the net air-sea heat flux. Equation (1) states that changes in heat content integrated over the cross-shelf area are caused by cross-shelf advection through the offshore side at $x = -L$, along-shelf heat flux divergence due to volume flux divergence and temperature gradient flux, and the net surface heat flux. In integrating to form (1), the vertical velocity is taken to be zero at the surface ($w = 0$ at $z = 0$) and given by the free slip kinematic boundary condition at the bottom ($w = -u\, \partial H/\partial x$ at $z = -H$), the cross-shelf heat flux is assumed to be zero at the coast (the vertical integral of $uT = 0$ at $x = 0$), and the heat flux through the seafloor is taken to be zero.

Equation (1) is useful because the cross-shelf integral of the cross-shelf heat flux is easily evaluated. However, as described by *Lentz* [1987b] and others, the addition of continuity to conservation of heat in (1) leads to a cross-shelf flux of temperature and along-shelf flux divergence of temperature which cancel when added together but depend on the absolute temperature scale when considered separately. In order to consider these terms separately, the velocity components u and v and temperature T in the cross-shelf and along-shelf volume flux divergence terms of (1) are decomposed into spatial average and perturbation quantities, for example,

$$\langle u \rangle = \frac{1}{H} \int_{-H}^{0} u|_{x=-L}\, dz \qquad (2)$$

and $u - \langle u \rangle = \bar{u}$. The angle brackets represent depth-averaged quantities at $x = -L$ for u and T and the cross-shelf area averaged quantity for v. Tildes represent departures from these spatial averages. Hence the quantities $\langle u \rangle$, $\langle T \rangle$, and $\langle v \rangle$ are functions of time only while $\bar{u}$, $\bar{T}$, and $\bar{v}$ depend on both space and time. Using this decomposition, (1) can be rewritten

$$\rho c_p \int_{-H}^{0} dx \int_{-H}^{0} \frac{\partial T}{\partial t}\, dz = \rho c_p \left[\int_{-H}^{0} \bar{u}\bar{T}|_{x=-L}\, dz - \int_{-L}^{0} dx \int_{-H}^{0} \bar{T} \frac{\partial v}{\partial y}\, dz - \int_{-L}^{0} dx \int_{-H}^{0} v \frac{\partial T}{\partial y}\, dz \right] + \int_{-L}^{0} Q\, dx \qquad (3)$$

where continuity has been used to eliminate the terms

$$H\langle u \rangle \langle T \rangle = \langle T \rangle \int_{-L}^{0} dx \int_{-H}^{0} \frac{\partial \langle v \rangle}{\partial y}\, dz \qquad (4)$$

Separating T, u, v, and Q in (3) into time mean (overbar) and fluctuating (prime) components and time averaging gives the mean heat budget equation. Using this decomposition, the mean cross-shelf heat flux is

$$\rho c_p \int_{-L}^{0} \overline{\bar{u}\bar{T}}\, dz = \rho c_p \left[\int_{-L}^{0} \overline{\bar{u}\bar{T}}\, dz + \int_{-L}^{0} \overline{\bar{u}'\bar{T}'}\, dz \right] \qquad (5)$$

The cross-shelf eddy heat flux in (5), $\overline{\bar{u}'\bar{T}'}$, is handled differently than in several previous papers [e.g., *Bryden et al.*, 1980; *Richman and Badan-Dangon*, 1983; *Send*, 1989]. Depth-averaged eddy heat flux terms are often not separated from the depth dependent flux terms, and the cross-shelf eddy heat flux is often written as

$$\int_{-H}^{0} \overline{u'T'}\, dz = \int_{-H}^{0} \overline{\bar{u}'\bar{T}'}\, dz + \int_{-H}^{0} \overline{\langle u \rangle' \langle T \rangle'}\, dz \qquad (6)$$

However, by (4) the cross-shelf, depth-averaged, eddy heat flux cancels the along-shelf, depth-averaged, eddy heat flux divergence in the same manner as the mean cross-shelf depth-averaged flux and along-shelf depth-averaged flux divergence cancel. Therefore we consider only the depth dependent cross-shelf eddy heat flux in the mean heat budget. The vertically integrated depth dependent fluxes in (3) are not a function of the absolute temperature scale. The vertical structures of the depth dependent fluxes do depend

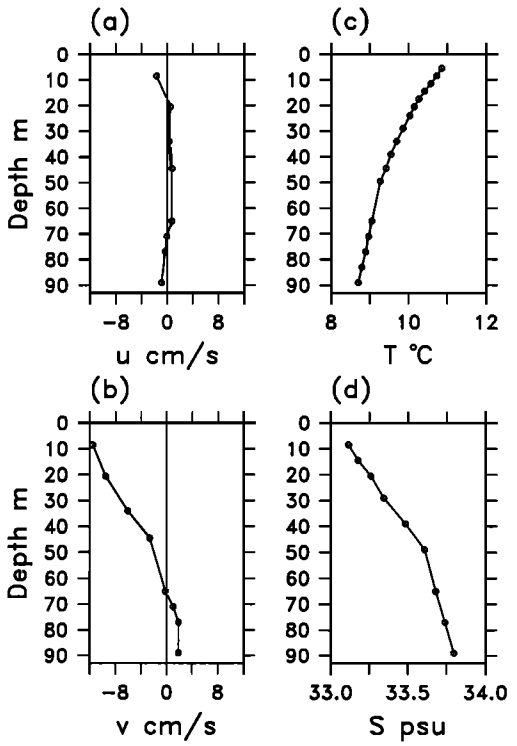

Figure 6. Mean (a) cross-shelf and (b) along-shelf velocity profiles at C3 between 2200 UT on March 3, 1989, and 0400 UT on May 2, 1989. Mean (c) temperature and (d) salinity profiles for the same time period are also shown. Means are only shown for depths (indicated by circles) with records lasting the entire time period. VMCM failures in the upper 49.5 m reduced near-surface velocity resolution during this time period.

on the temperature scale, but they remain similar and have sensible interpretations provided temperature is measured relative to an average such as the depth or cross-shelf area average. The approach of separating the depth dependent components of the heat budget is the two-dimensional analog to the method used to compute heat fluxes over a volume by *Lentz* [1987b].

3.2. Estimation of Terms in the Mean and Low-Passed Heat Budgets

Terms in a time mean and a 38-hour low-passed (using the PL64 filter described by *Limeburner* [1985]) version of (3) were estimated using time series of u, T, and v at C3 and T at G3 and M3. At deployment time, temperature and velocity observations existed at common depths at C3; however, current meter failures (see Figure 3) necessitated interpolation of velocity components at about half the temperature sensor depths for at least a portion of the time series. It was also necessary to extrapolate above and below the shallowest and deepest observations to the surface and bottom. Because vertical length scales of variability were much greater than the instrument separations, interpolated values were insensitive to the particular interpolation scheme, and we chose linear interpolation. Extrapolation of current and temperature information from the shallowest VMCM (at 8.5 m or 5.5 m) to the surface was more problematic. We chose to extrapolate above and below the shallowest and deepest functioning sensor depths assuming a vertically uniform profile.

In winter, uniform extrapolation of u between 5.5 m and the surface and between 91 m and the bottom yielded similar results as more complicated extrapolation schemes, despite winter near-surface and near-bottom current data during SMILE and STRESS [*Santala*, 1991; *Gross et al.*, 1992] which suggest this is an oversimplification. For example, linear extrapolation above the shallowest and below the deepest observations changed mean winter values of the cross-shelf heat flux by only 10%. Uniform extrapolation probably did well because the surface boundary layer, as indicated by mean and median surface mixed layer (SML) depths of 16 and 14.5 m (estimated following *Lentz* [1992]), was resolved by several current meters; hence it was not solely dependent on transport above 5.5 m. This is supported by a comparison of the low-passed SML to surface Ekman transport, $\tau_y/\rho f$, which shows they are correlated at the 99.9% level (correlation coefficient 0.71) with a regression coefficient of SML transport on Ekman transport of 0.78.

In spring, uniform extrapolation of current and temperature above the shallowest observations almost certainly resulted in some underestimate of the cross-shelf heat flux. The mean SML depth in spring was 6 m, and over half the SML depth estimates were 0 m, suggesting the surface boundary layer was not well resolved by functioning current meters. This is also indicated by a comparison of low-passed SML transport to the low-passed surface Ekman transport which shows that though they are still correlated at the 99.9% level (correlation coefficient 0.78), the regression coefficient of SML transport on Ekman transport is 1.45 in spring. Inclusion of a transition layer below the SML, as suggested by *Lentz* [1992], did not account for this discrepancy. Though linear extrapolation above 8.5 m increased the spring mean offshore heat flux by almost a factor of 2, only uniform extrapolation results are presented because uniform extrapolation was consistent with the winter analysis, and because the absence of current measurements above 8.5 m during most of spring made all extrapolation schemes untestable.

After interpolating and extrapolating current observations to the C3 temperature depths, components of the mean and fluctuating heat budgets were calculated. The depth dependent cross-shelf velocity $\bar{u}$ was calculated by subtracting the depth-averaged cross-shelf velocity $\langle u \rangle$ (found by trapezoidally integrating u and dividing by the depth, 93 m) from u at each observation depth. Depth dependent temperature time series $\bar{T}$ were estimated in the same way. The low-passed time series of cross-shelf heat flux was calculated by multiplying the hourly time series of the $\bar{u}$ and $\bar{T}$ together, vertically integrating them, and low-pass filtering the result. The mean cross-shelf heat flux was estimated from the unfiltered cross-shelf heat flux time series, and the cross-shelf eddy heat flux was calculated by vertically integrating the covariance of $\bar{u}$ and $\bar{T}$.

To estimate the change in heat content over the cross-shelf area, time series of $\partial T/\partial t$ were computed at each C3 depth using centered differences of hourly observations. Because there were no temperature measurements between C3 and the coast in winter, heat content was assumed to be uniform from C3 to the coast. To estimate heat gain or loss over the cross-shelf area, the time derivatives of temperature at each depth were multiplied by the estimated cross-shelf distance from C3 to the isobath equal to each measurement depth and vertically integrated. Time-averaged and low-pass-filtered changes in heat content were derived from the hourly time series. The assumption that heat content changes were uniform in the cross-shelf direction was checked for the upper 49.5 m in spring using the C2 mooring. C2 was deployed just prior to the beginning of the spring time period and was halfway between the C3 mooring and the coast (Figure 2). Because of near-shore warming, inclusion of the C2 mooring increased the estimate of mean heat content change in spring by about one third but did not alter the fundamental balances of the spring mean and fluctuating heat budgets discussed in section 5. For this reason, and because cross-shelf temperature information was unavailable below 49.5 m in spring, we chose to present estimates for cross-shelf integrated heat content change based on the C3 mooring alone for both winter and spring.

The net surface heat flux at C3 was estimated from bulk formulas using hourly meteorological measurements at C3 and nearby locations. It was assumed spatially uniform and was multiplied by the distance to the coast, 6.3 km, to get the cross-shelf integrated sea surface flux. The hourly time series was then averaged and low-pass filtered to give mean and fluctuating air-sea heat fluxes. The procedure for estimating the sea surface flux and a discussion of uncertainties are given in Appendix A.

Lack of information about spatial variability of along-shelf velocity and temperature made estimates of along-shelf heat flux divergence subject to strong assumptions. The along-shelf heat flux divergence in (3) is given by

$$-\rho c_p \int_{-L}^{0} dx \int_{-H}^{0} v \frac{\partial T}{\partial y} dz \qquad (7)$$

the heat flux divergence caused by along-shelf advection of an along-shelf temperature gradient, and

$$-\rho c_p \int_{-L}^{0} dx \int_{-H}^{0} \tilde{T} \frac{\partial v}{\partial y} dz \qquad (8)$$

the heat flux divergence caused by the along-shelf volume transport divergence. Following *Richman and Badan-Dangon* [1983], (7) is called the along-shelf temperature gradient flux. It was estimated from temperature observations at G3 and M3 and velocity measurements at C3. The along-shelf temperature gradient in the upper 49.5 m at C3 was estimated by differencing G3 and M3 temperatures and dividing by the along-shelf distance, 29.2 km. G3 and M3 temperatures were linearly interpolated to the same depths as the C3 observations where necessary. To estimate the along-shelf temperature gradient flux, the along-shelf temperature gradient was multiplied by the along-shelf velocity at C3. Gaps in along-shelf velocity observations were filled following the same interpolation/extrapolation procedure used on the cross-shelf velocity. In the absence of other information the along-shelf temperature gradient flux was assumed to be uniform in x so that the integral of $v\ \partial T/\partial y$ in the cross-shelf direction was estimated by multiplying by the distance to the coast at each depth. This was vertically integrated from 49.5 m to the surface. Mean, eddy, and fluctuating components of the along-shelf temperature gradient flux were estimated as for the cross-shelf heat flux. Observations of along-shelf velocity at C2 in spring and of the cross-shelf structure of temperature, along-shelf velocity, and along-shelf heat flux in summer [*Winant et al.*, 1987; *Lentz*, 1987b] indicate the assumption of uniformity in x is an oversimplification. However, the sign and magnitude of the along-shelf temperature gradient flux as estimated above are consistent with other information in both the time mean and the fluctuating heat budgets.

Unfortunately, the depth dependent along-shelf heat flux divergence in (8) cannot be even crudely estimated because $\partial v/\partial y$ is unknown. We feel it is unlikely that (8) dominates the winter heat budget given its near closure. However, (8) may play a significant role in spring when the heat balance does not close as well and circumstantial evidence indicates the presence of mesoscale features.

3.3. Estimating the Mean and Low-Passed Salt Budgets

Conductivity time series measured at the central SMILE and STRESS moorings allowed some terms in the salt budget to be estimated and compared to the heat budget. The salt balance used was analogous to (3), and terms in the salt budget were estimated in the same manner as those in the heat budget. To gauge qualitatively the effects of the reduced vertical resolution of salinity measurements relative to temperature measurements, the heat budget was recalculated at the same reduced resolution as the salt budget. Vertically integrated values for cross-shelf fluxes and heat content changed by roughly 10%, but the basic balances did not. The lack of along-shelf salinity time series measurements meant along-shelf salinity fluxes could not be estimated. The mean net freshwater surface flux was estimated from evaporation based on the latent heat flux at C3 and precipitation from a coastal rain gauge at Stewart's Point (see Figure 1). Other rainfall measurements taken during SMILE show this rain gauge is representative of rainfall extending northward approximately 90 km to Cabrillo Point [see *Alessi et al.*, 1991, Figure 32].

4. Results

4.1. Mean Winter and Spring Heat Budgets

Using the methods developed in section 3, we summarize the vertically integrated winter and spring heat balances per unit along-shelf distance in Tables 1 and 2. In both winter and spring the mean cross-shelf heat flux, though about a factor of 5 smaller than in summer, is a dominant term in the mean heat budget. Tables 1 and 2 show it is largely the result of the mean advection of the mean temperature field (Figures 5 and 6). Mean cross-shelf velocities are highest in the surface and bottom boundary layers. This leads to the vertical structures in Figures 7 and 8 which show a near-surface offshore maximum caused by the offshore flow of the warmest water on the shelf and a near-bottom onshore maximum caused by the offshore flow of the coldest water on the shelf. Though the general character of the vertical structures of the winter and spring cross-shelf heat flux is similar, they differ in detail. In winter the near-surface offshore heat flux extends to 25 m. In spring, near-surface offshore heat flux values are larger than in winter but are confined to the top 10 m. This is due to a stronger spring near-surface stratification and near-surface offshore mean flow only above 10 m in spring. The highly surface-intensified structure of the spring mean cross-shelf flux is a further suggestion that it may be underestimated, since the top velocity sensor (at 8.5 m during most of this time) is only barely within the near-surface region. The near-bottom offshore heat transport is consistent with Ekman bottom boundary layer dynamics in that observed interior poleward flow is associated with offshore near-bottom flow (the correlation between v at 67 m and u at 91 m, -0.45, is significant at the 99% level).

The other advective contribution to the mean heat budgets, the along-shelf temperature gradient flux, is the second largest component of the winter mean heat budget and the third largest component of the spring mean heat budget. Tables 1 and 2 show this term (especially in winter) is largely the result of an eddy along-shelf temperature gradient flux, not of a mean advective flux. Though the magnitude of the along-shelf temperature gradient flux should be viewed skeptically, since its estimation is subject to strong assumptions,

Table 1. Estimated Terms in Winter 1988–1989 Heat and Salt Balances

	Mean	Eddy Contribution to Mean	Standard Error	Standard Deviation
Heat content change*	−2.8	···	5.0	33.8
Cross-shelf heat flux*	−8.7	1.5	3.7	25.3
Along-shelf temperature gradient flux†	5.1	5.2	1.9	10.6
Air-sea heat flux*	0.1	···	0.5	3.6
Heat balance residual†	−0.6	···	4.6	25.5
Salt content change*	7.9	···	44.1	299.4
Cross-shelf salt flux*	147.9	3.0	45.5	308.9

Heat budget units are in 10^5 W m^{-1}, and salt budget units are in 10^{-3} m^2 psu s^{-1}. Standard error estimates are calculated from low-passed data with the number of independent observations found from the record hours divided by an integral time scale.

*Standard error assumes integral timescale of 40 hours.

†Standard error assumes integral timescale of 60 hours.

Table 2. Estimated Terms in Spring 1989 Heat and Salt Balances

	Mean	Eddy Contribution to Mean	Standard Error	Standard Deviation
Heat content change*	3.1	···	6.4	38.0
Cross-shelf heat flux*	−6.4	1.1	7.2	42.7
Along-shelf temperature gradient flux†	4.3	2.9	2.8	13.7
Air-sea heat flux*	8.3	···	0.9	5.2
Heat balance residual†	3.2	···	8.7	42.2
Salt content change*	−32.4	···	60.4	360.1
Cross-shelf salt flux*	41.7	−13.9	60.0	357.9

Heat budget units are in 10^5 W m^{-1}, and salt budget units are in 10^{-3} m^2 psu s^{-1}. Standard error estimates are calculated as in Table 1.

*Standard error assumes integral timescale of 40 hours.

†Standard error assumes integral timescale of 60 hours.

the negative correlation coefficients associated with the eddy along-shelf temperature gradient flux in winter were greater than −0.30 (the 95% significance level), suggesting that stronger than average poleward flow was associated with equatorward temperature gradients and vice versa at C3. During spring this correlation coefficient is weaker, and the mean advection of the mean temperature gradient became about half as large as the eddy along-shelf temperature gradient flux. The mean along-shelf temperature gradient

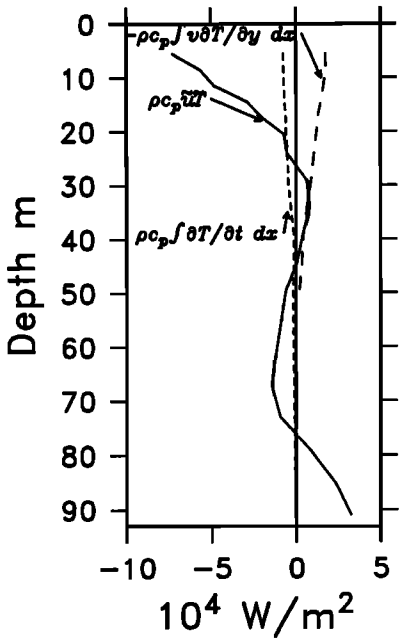

Figure 7. Vertical profiles of the three largest terms in the 1988–1989 mean winter heat budget. The mean cross-shelf heat flux is indicated by the solid line, the local heat content change by the short-dashed line, and the along-shelf temperature gradient flux by the long-dashed line. The mean cross-shelf heat flux is almost entirely the result of the mean advection of the mean temperature field. In contrast, the mean along-shelf temperature gradient flux is almost entirely due to eddy along-shelf temperature gradient flux.

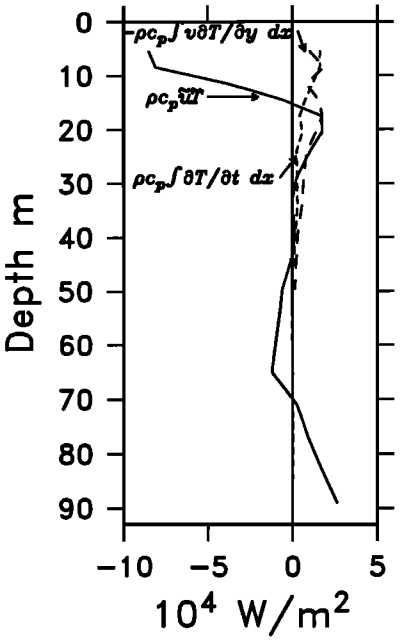

Figure 8. Profiles of terms in the mean spring heat budget. The mean cross-shelf heat flux is indicated by the solid line, the local heat content change by the short-dashed line, and the along-shelf temperature gradient flux by the long-dashed line. The largest single component of the mean spring heat flux is the mean surface heat flux (not shown).

flux is greatest near the surface and decreases monotonically with depth. This decrease is primarily due to larger near-surface values of along-shelf temperature gradient flux rather than to the smaller cross-shelf area represented by deeper observations.

It is in the air-sea heat flux that winter and spring show the greatest difference. In winter its contribution to the mean heat budget is an order of magnitude smaller than the largest estimated terms (Table 1), but in spring it becomes the single largest term in the mean heat budget (Table 2). This was due to an increase in incoming shortwave radiation from an average of 104 W m^{-2} in winter to 190 W m^{-2} in spring and a decrease in the latent heat flux from an average of −39 W m^{-2} in winter to −18 W m^{-2} in spring.

As a result of these processes, the local heat content decreases in winter and increases in spring. Winter in situ cooling corresponded to a depth-averaged temperature drop at C3 of about 1.0°C over a 77-day period. The winter change in mean heat content is largest near the surface and decreases with depth. Above 60 m this decrease was due primarily to larger near-surface mean values of in situ cooling, and below 60 m it was due to the smaller cross-shelf area represented by near-bottom observations. Spring in situ heating would correspond to a depth-averaged temperature increase at C3 of about 1.1°C over a 59-day period, but this increase occurred primarily in the upper 20 m with little change in heat content below this depth.

Our analysis has shown that the mean winter and spring balances are qualitatively different. In winter the absence of surface heating leads to a three-dimensional balance between the negative cross-shelf heat flux and the positive along-shelf temperature gradient flux. In spring, surface heating is a major term in the mean heat balance, which is

primarily between surface heating and a negative cross-shelf heat flux. In both winter and spring the mean cross-shelf heat flux is due to the mean advection of the mean temperature field and has a vertical structure consistent with a wind-forced surface boundary layer and an along-shelf velocity-forced bottom boundary layer. In contrast, the along-shelf temperature gradient flux is due to an eddy gradient flux, rather than to mean along-shelf advection.

4.2. Fluctuating Heat Budgets

Fluctuations in the low-pass-filtered heat budget (Figures 9 and 10) are 1–2 orders of magnitude larger than means (in Tables 1 and 2). In contrast to the mean heat budgets, the dominant balance in the fluctuating heat budgets at periods of days to weeks was

$$\int_{-L}^{0} dx \int_{-H}^{0} \frac{\partial T}{\partial t}\, dz = \int_{-H}^{0} \tilde{u}\tilde{T}\, dz \qquad (9)$$

The along-shelf temperature gradient flux was only occasionally important at these time scales, and air-sea heat flux only

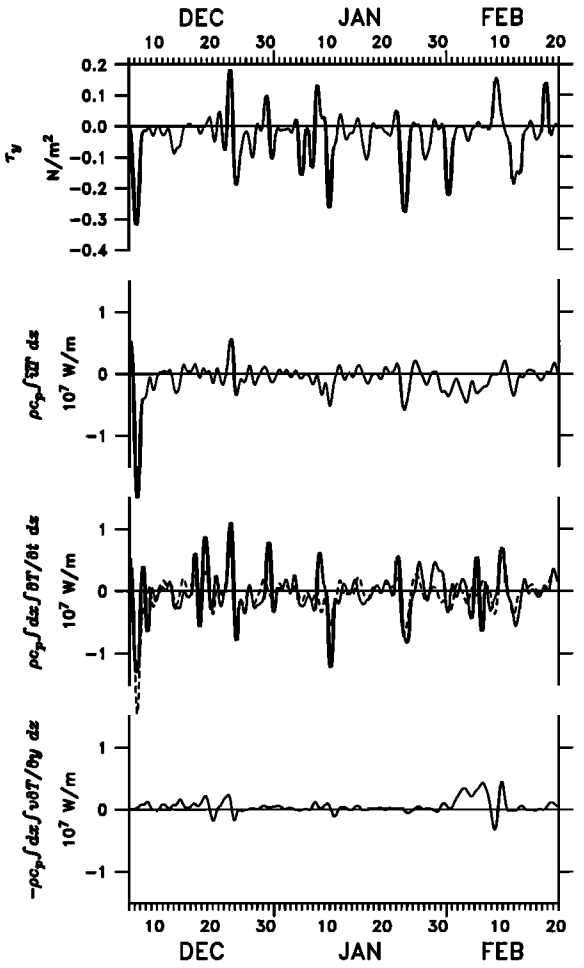

Figure 9. Low-passed time series of along-shelf wind stress and terms in the depth-integrated winter heat budget. Zero-lag correlations of terms are given in Table 3. The dashed line in the third plot from the top is the sum of the cross-shelf heat flux, along-shelf temperature gradient flux, and net air-sea heat flux. The correlation between this sum and the estimated heat content change is 0.67.

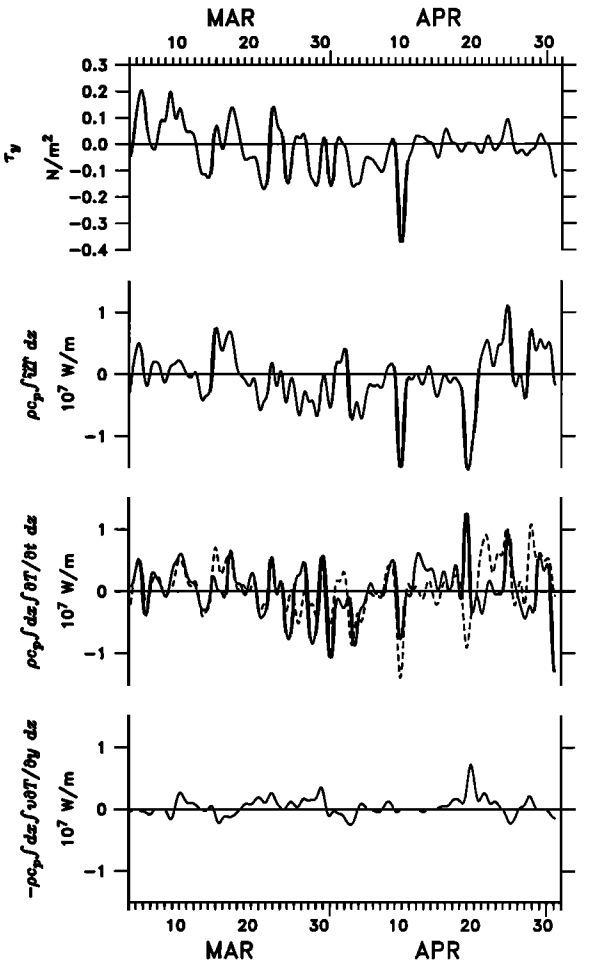

Figure 10. Low-passed time series of along-shelf wind stress and terms in the depth-integrated spring heat budget. The dashed line in the third plot from the top is the sum of the cross-shelf heat flux, along-shelf temperature gradient flux, and net air-sea heat flux. The correlation between this sum and the estimated heat content change is 0.39. Other zero-lag correlations are given in Table 4.

became appreciable at time scales of 1 month or longer in spring (Figures 11 and 12). The correlations of terms in (9) with each other and with the low-passed along-shelf wind stress at C3 (Tables 3 and 4) indicate that the likely physical process accounting for the balance represented in (9) was the response of the cross-shelf heat transport and temperature to local along-shelf wind forcing. The lower spring correlation coefficients may be caused by a lack of velocity information above 8.5 m, weak wind forcing in April, and/or the presence of a mesoscale feature over the northern California shelf during this time [*Largier et al.*, 1993]. On an event basis, examination of Figures 9–12 shows episodic removal of heat from the shelf occurring on five occasions (December 7, December 24, January 11, January 24, and April 10) following equatorward wind stresses of 0.2 N m^{-2} or greater, several short-lived increases in heat content associated with poleward winds immediately preceding winter upwelling events, and a longer increase in heat content during poleward wind stresses for several weeks in March. This last increase in heat appears similar in character to the removal of heat caused by upwelling events in winter. It does not

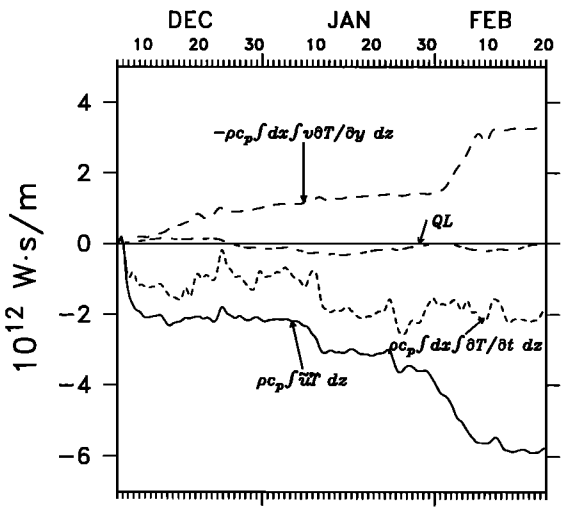

Figure 11. Time-integrated change in heat content at C3 through the winter. The heat content change is indicated by the short-dashed line, the change due to cross-shelf advection by the solid line, that due to along-shelf advection by the long-dashed line, and that due to surface heating by the alternately long-dashed, short-dashed line. A change of 10^{12} W s m^{-1} corresponds to a change in the depth-averaged temperature of 0.54°C.

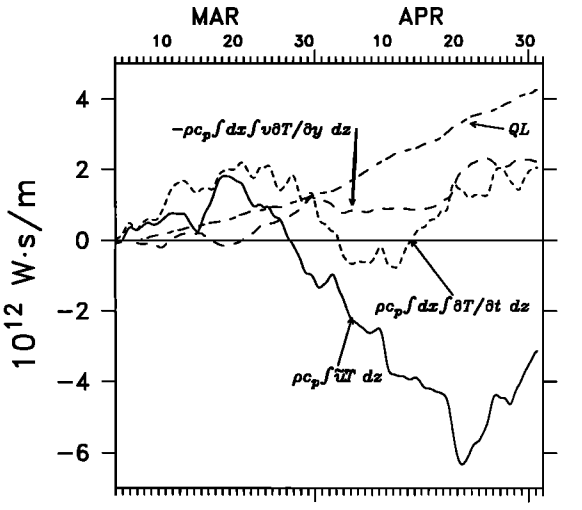

Figure 12. Time-integrated change in heat content at C3 through the spring. The heat content change is indicated by the short-dashed line, the change due to cross-shelf advection by the solid line, that due to along-shelf advection by the long-dashed line, and that due to surface heating by the alternately long- and short-dashed line. A change of 10^{12} W s m^{-1} corresponds to a change in the depth-averaged temperature of 0.54°C.

show that upwelling and downwelling are symmetric, though it does indicate that the short-lived upwelling/downwelling events prior to the transition to upwelling season may have similar effects on the fluctuating heat budget.

To examine the vertical structure of the low-passed heat balance, covariance empirical orthogonal functions (EOFs) were formed from the low-passed time series of heat content change, along-shelf temperature gradient flux, and cross-shelf heat flux. The vertical structure of the lowest EOF of the fluctuating cross-shelf heat flux (Figures 13 and 14) has near-surface and near-bottom maxima in the same direction, unlike the mean cross-shelf heat flux (Figures 7 and 8) which has offshore flow of cool water in the bottom boundary layer caused by the mean poleward flow. Figures 13 and 14 suggest a two-dimensional conceptual model with offshore flow of relatively warm water in a wind-driven surface boundary layer and onshore return flow of cooler water in the interior and in the bottom boundary layer. Like the depth-integrated time series, the lowest EOF amplitude time series of heat content change are correlated with the cross-shelf heat fluxes above the 99% level (correlation coefficient of 0.56 (0.49) in winter (spring)), and both are correlated with the wind stress (0.64 (0.61) for heat content change and 0.63 (0.69) for cross-shelf heat flux).

Along-shelf temperature gradient flux usually made a secondary contribution to the fluctuating heat budgets. It was not correlated with the along-shelf wind stress and became evident during several events lasting 2–3 weeks in December, early February, March, and late April (Figures 9 and 10), factors which suggest it may be due to mesoscale features. The lowest EOF (Figures 13 and 14) of the along-shelf temperature gradient flux is surface intensified, and its amplitude time series shows that all instances of large along-shelf temperature gradient flux are surface intensified. In at least two events (February and April) the positive contribution of the along-shelf temperature gradient flux acts to balance a simultaneous negative cross-shelf heat flux. However, in the spring event of April 20–26, estimates of heat content change do not agree well with the sum of cross-shelf heat flux, along-shelf temperature gradient flux,

Table 3. Low-Passed Correlation Coefficients for Winter 1988–1989 Heat and Salt Balances

	Along-Shelf Wind Stress	Heat Content	Cross-Shelf Heat Flux	Along-Shelf Temperature Gradient Flux	Salt Content	Cross-Shelf Salt Flux
Along-shelf wind stress	1	0.68	0.64	0.14	−0.69	−0.60
Heat content		1	0.59	0.21	−0.71	−0.53
Cross-shelf heat flux			1	−0.08	−0.57	−0.80
Along-shelf temperature gradient flux				1	−0.18	0.27
Salt content					1	0.53
Cross-shelf salt flux						1

Zero-lag correlation coefficients were very near maximum lagged correlations. For a 40-hour integral timescale (used for wind stress, heat (salt) content changes, and cross-shelf heat (salt) fluxes), correlations of 0.20, 0.30, and 0.39 are significant at the 80%, 95%, and 99% levels, respectively. For a 60-hour integral timescale (used for correlations involving along-shelf temperature gradient fluxes), correlations of 0.24, 0.36, and 0.46 are significant at the 80%, 95%, and 99% levels, respectively.

Table 4. Low-Passed Correlation Coefficients for Spring 1989 Heat and Salt Balances

	Along-Shelf Wind Stress	Heat Content	Cross-Shelf Heat Flux	Along-Shelf Temperature Gradient Flux	Salt Content	Cross-Shelf Salt Flux
Along-shelf wind stress	1	0.65	0.60	0.00	−0.57	−0.61
Heat content		1	0.35	0.06	−0.74	−0.39
Cross-shelf heat flux			1	−0.36	−0.15	−0.95
Along-shelf temperature gradient flux				1	−0.36	0.33
Salt content					1	0.24
Cross-shelf salt flux						1

Integral timescales are as in Table 3. Correlations of 0.23, 0.35, and 0.45 are significant at the 80%, 95%, and 99% levels, respectively, for correlations between wind stress, heat (salt) content change, and cross-shelf heat (salt) flux. Correlations of 0.28, 0.41, and 0.53 involving along-shelf temperature gradient flux are significant at the 80%, 95%, and 99% levels, respectively.

and air-sea heat flux, which may indicate that the along-shelf heat flux divergence contained in (8) is important during this time.

The fluctuating balances in both winter and spring are predominantly between heat content change and cross-shelf heat fluxes. These are well correlated with the wind, and the fluctuating cross-shelf heat flux has a vertical structure determined by wind-driven surface and bottom boundary layers. The along-shelf temperature gradient flux is only secondarily important. It is not correlated to the wind, may result from poleward advection of an equatorward temperature gradient or vice versa, and is probably due to mesoscale features. The air-sea heat flux is not important to the fluctuating winter heat budget and becomes important on time scales of 1 month to the spring heat balance.

4.3. Salt Budget

In general, the salt balance was similar to the heat balance. The largest term in the mean salt balances (Tables 1 and 2) was the onshore salt flux. Its vertical structure (shown only for winter in Figure 15) was essentially a mirror image of the vertical structure of the mean cross-shelf heat flux (Figures 7 and 8), suggesting that it was caused by a mean offshore advection of low-salinity water near the surface. Other estimated terms in the mean salt balance were much smaller than the mean cross-shelf salt flux which, in the absence of other processes, would increase salinity about +2.18 psu in winter and +0.47 psu in spring. In winter the observed mean salinity change was much less, about +0.12 psu, and in spring the mean salinity change was actually −0.37 psu. The net surface freshwater flux could have offset the cross-shelf flux by only 0.04 (0.11) psu in winter (spring). This imbalance suggests that an along-shelf salt flux divergence closed the mean salt budgets. It is possible that this along-shelf salt divergence was a result of river runoff from the Russian River south of C3 (Figure 1), but even in the absence of river runoff the mean temperature-salinity (T-S) relationship (Figure 16) suggests that the mean along-shelf temperature

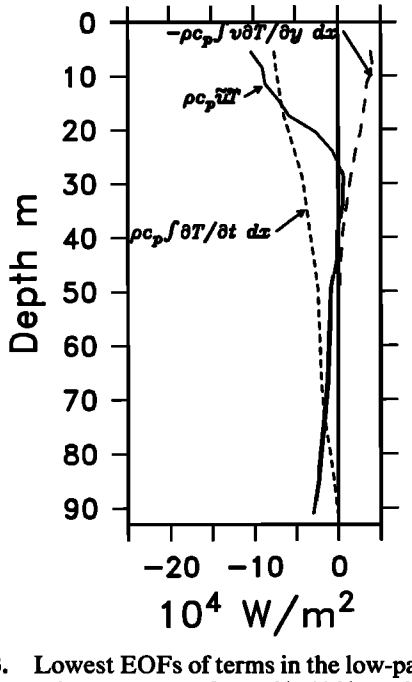

Figure 13. Lowest EOFs of terms in the low-passed winter heat budget. These account for 79%, 77%, and 86% of the cross-shelf heat flux (solid line), local heat content (short-dashed line), and along-shelf temperature gradient flux (long-dashed line) variance, respectively.

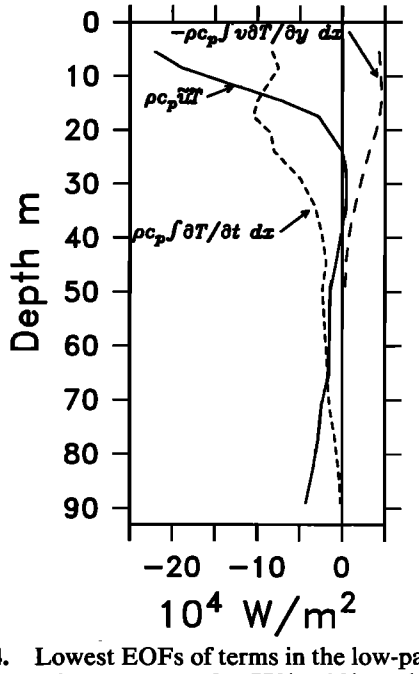

Figure 14. Lowest EOFs of terms in the low-passed spring heat budget. These account for 77%, 62%, and 81% of the cross-shelf heat flux (solid line), local heat content (short-dashed line), and along-shelf temperature gradient flux (long-dashed line) variance, respectively.

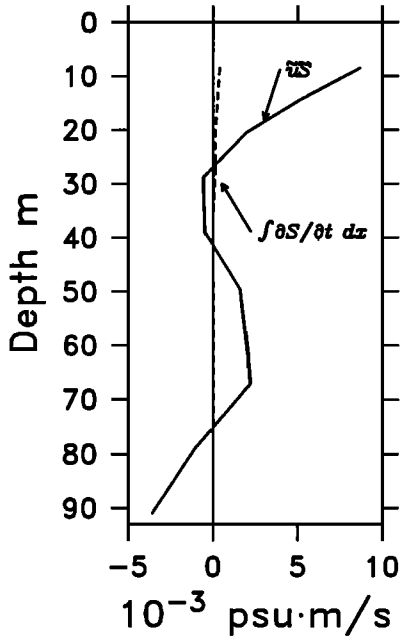

Figure 15. Salt flux profiles of terms in the mean winter salt budget. The mean cross-shelf salt flux is indicated by the solid line, and the local salt content change by the dashed line.

gradient flux at C3 would be associated with a negative contribution to the salt balance.

To gauge qualitatively whether along-shelf salinity gradients were associated with along-shelf temperature gradients, observations from three SMILE conductivity-temperature-depth (CTD) cruises [*Limeburner and Beardsley*, 1989a, b, c] in November 1988, February through March 1989, and May 1989 were compared with simultaneous C3 mooring temperatures and salinities. The cruises included repeated surveys and along-shelf sections with a total of 92 stations along the 93-m isobath with roughly 15 km resolution. Along-shelf temperature and salinity differences were negatively correlated with a correlation coefficient of −0.59. Assuming each CTD survey or along-shelf section represented an independent observation (time evolution was rapid enough that individual surveys lasting 1 or 2 days could not be considered synoptic), this correlation coefficient is significant at the 95% level. The negative correlation coefficient indicates that a poleward transport of low-salinity water would be associated with a poleward transport of heat and vice versa.

Like the mean salt balance, the low-passed fluctuating salt balance provided essentially the same information as the low-passed heat balance. Cross-shelf heat and salt fluxes are negatively correlated (Tables 3 and 4), as are changes in heat and salt content. Changes in salinity and the cross-shelf salt flux are well correlated to each other and to the along-shelf wind stress. The lowest EOF modes of vertical structure for salt content and cross-shelf salt flux are very similar to, and negatively correlated with, those of heat content (correlation coefficients −0.70 and −0.60 in winter and spring, respectively) and cross-shelf heat flux (correlation coefficients −0.79 and −0.93 in winter and spring, respectively). The periods when cross-shelf salt flux and changes in salt content agree least correspond to the periods when the along-shelf temperature gradient flux was important, a further indication that the along-shelf salt flux divergence is related to the along-shelf temperature gradient flux.

5. Discussion and Summary

Mean and fluctuating heat and salt budgets per unit along-shelf distance have been estimated using measurements from the 1988–1989 SMILE/STRESS field programs for the northern California shelf. On the basis of data coverage and the absence or presence of persistent surface heating, these time series have been analyzed as two distinct periods: a winter period characterized by weak surface heating and a spring period during which surface heating is important. Both winter and spring were subject to weak mean winds, making meteorological conditions different from summer upwelling season, which began immediately after the end of the spring time period in 1989. The goals of this discussion are to contrast the winter and spring heat budgets with those observed in the summer upwelling season on the northern California shelf and elsewhere and to put our results in the context of climatological forcing conditions.

One of several points which stand out in comparing the mean winter, spring, and summer upwelling heat balances is the relative magnitudes of terms in the balances. To compare the winter and spring heat budgets per unit along-shelf distance to the volume heat budget of *Lentz* [1987b], the heat content change and along-shelf heat flux divergence values reported by Lentz were divided by his study volume of 79.1 km^3 and multiplied by the cross-shelf area between CODE C3 and the coast, 0.39 km^2. Similarly, the cross-shelf heat flux values were divided by the along-shelf distance, 56 km; the net air-sea heat flux was divided by the surface area of 936 km^2 and multiplied by the distance between CODE C3 and the coast, 5.8 km. The mean cross-shelf heat flux and net air-sea heat flux are directly dependent on the persistence of upwelling favorable winds and seasonal variation in solar

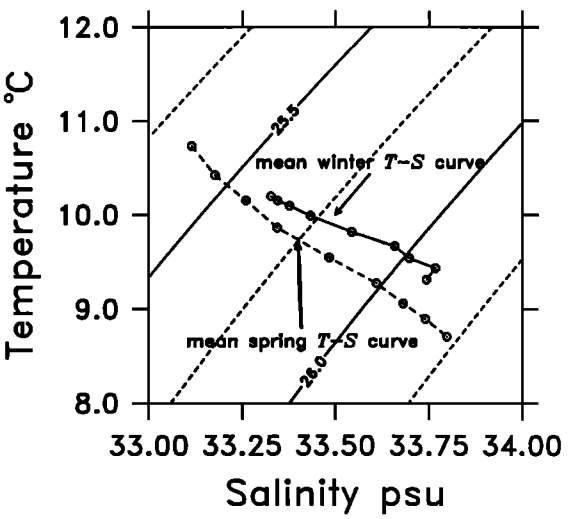

Figure 16. Mean *T-S* relation at C3 in winter (solid curve) and spring (dashed curve). Surface mooring observation depths were at 8.5, 14.5, 20.5, 29.0, 39.0, and 49.5 m. Subsurface mooring observation depths were at 67, 79, and 91 m in winter and 65, 77, and 89 m in spring.

insolation. Therefore they show the greatest variations in magnitude between winter, spring, and summer. The mean cross-shelf heat fluxes per unit along-shelf distance in winter and spring (Tables 1 and 2) are about a factor of 5 smaller than the estimated summer value on the northern California shelf of -42.3×10^5 W m^{-1}. The mean net air-sea heat flux also shows large variability; it increases from winter and spring values (Tables 1 and 2) to 10.0×10^5 W m^{-1} in summer. By contrast, the summer mean along-shelf temperature gradient flux (a portion of the total heat flux divergence) and heat content change (-2.7×10^5 W m^{-1} and -2.4×10^5 W m^{-1}, respectively) have magnitudes similar to those in winter and spring (Tables 1 and 2).

These changes in relative magnitude lead to differences in the character of winter, spring, and summer mean heat balances. The winter heat balance is between the negative mean cross-shelf heat flux and positive along-shelf temperature gradient flux, making it three dimensional to the lowest order. The mean spring and summer heat balances are between the negative cross-shelf heat flux and the positive net air-sea heat flux, making them more two dimensional in character. However, the cross-shelf heat flux is much weaker in spring than in summer, so that a mean increase in heat content occurs in spring, rather than the slight decrease observed in summer upwelling season.

Regardless of the season, the mean cross-shelf heat flux is of importance to the mean heat balance. The most prominent characteristic of its vertical structure in winter and spring, a near-surface offshore heat flux, is similar to that observed in upwelling systems off Oregon [*Bryden et al.*, 1980], northwest Africa [*Richman and Badan-Dangon*, 1983], and northern California [*Lentz*, 1987b]. Below the surface the winter and spring mean cross-shelf heat fluxes decrease in magnitude and have a sign which varies with depth. Near the bottom the winter and spring cross-shelf heat fluxes are stronger and onshore because of the offshore flow of the coldest water on the shelf. *Richman and Badan-Dangon* [1983] also observed a near-bottom increase in cross-shelf heat transport magnitude on the northwest African shelf, though it was offshore because of onshore transport of cold water. The directions of near-bottom cross-shelf heat transport found by *Richman and Badan-Dangon* [1983] and this study can be explained by a near-bottom Ekman transport driven by a mean interior along-shelf flow. *Bryden et al.* [1980] and *Lentz* [1987b] find no near-bottom increase in cross-shelf heat transport, possibly because the bottom boundary layer, expected to be thin during active upwelling events [*Weatherly and Martin*, 1978; *Trowbridge and Lentz*, 1991], was not resolved with available measurements. The mean winter and spring cross-shelf heat flux vertical structures are consistent with the notion that mean winds, though weak, drive an offshore flow of relatively warm water in the surface boundary layer and poleward along-shelf currents set up an offshore flow of the coldest water in the bottom boundary layer.

Though mean heat budgets observed in winter, spring, and summer are quite different, fluctuating heat budgets are similar. The magnitude of the fluctuations in winter and spring are within a factor of 2 of fluctuations in the summer upwelling budget [*Lentz*, 1987b]. In all three cases the dominant balance is between the cross-shelf heat flux and local changes in heat content. These terms are highly correlated with the local along-shelf wind stress and each other (this is true to a lesser degree in spring). The vertical structure of the fluctuating cross-shelf heat flux, as represented by the lowest EOF mode, suggests wind-driven surface and bottom boundary layers. Thus it appears that short-timescale variability is dominated by a wind-driven cross-shelf heat flux with a resulting change in heat content in winter, spring, and summer [*Lentz*, 1987b; *Lentz and Chapman*, 1989]. It is interesting to note that poleward winds associated with downwelling can result in a shoreward flux of heat and an increase in heat content. In this respect at least, downwelling events appear to be similar to upwelling events in winter and spring.

This two-dimensional picture of the fluctuating heat budget is upset in February, March, and late April when the along-shelf temperature gradient flux becomes important on time scales of weeks. During these times the along-shelf temperature gradient flux tends to be offset by the cross-shelf heat flux, reducing the net change in heat content. *Lentz* [1987b] found a similar event in the 1982 summer upwelling heat budget which he attributed to the presence of an offshore mesoscale feature seen in satellite infrared images. The events in February, March, and April 1989 do not appear to be locally wind driven and may also be due to mesoscale features. *Largier et al.* [1993] also observed mesoscale features over the northern California shelf and slope in March and April 1989 during the Northern California Coastal Circulation Study (NCCCS), a field program designed to study large-scale circulation.

The mean heat balances in winter 1988–1989 and spring 1989 differ to varying degrees from summer upwelling balances which are thought to be relatively robust. However, even the largest terms in the mean balances (Tables 1 and 2), with the exception of the spring air-sea heat flux, are scarcely larger than their standard errors. One question which then arises is how general are the 1988–1989 mean balances? To help answer this question, we constructed a heat balance from more limited data taken in the winter of 1981–1982 (Appendix B). This analysis yielded mean (and fluctuating) balances very similar to those in the winter of 1988–1989; hence it provided some confidence in the generality of 1988–1989 results. However, the along-shelf wind stress, the net air-sea heat flux, and the along-shelf velocity, all important factors in determining the winter and spring heat balances, are likely to vary significantly over the course of a single season as well as between seasons and geographically. Because the dominant terms in the mean winter and spring heat balances have small magnitudes compared to their fluctuations, variation in these forcing factors may alter the magnitude or even the sign of individual terms in the mean winter and spring heat balances.

The most important factor in determining the cross-shelf heat flux, the along-shelf wind stress, is less uniform in time and space than in summer when winds are generally upwelling favorable. *Nelson* [1977] and *Strub et al.* [1987a] show seasonal along-shelf winds to be equatorward all along the Washington, Oregon, and California coasts during summer months but spatially variable in winter months, becoming poleward north of 39°N, remaining equatorward south of this latitude, and becoming weak and variable off northern California. The locations of both the SMILE and the CODE field programs are near this latitude where the sign and magnitude of a mean winter or spring along-shelf wind stress may be expected to vary. Figure 17, the 30-day low-pass-

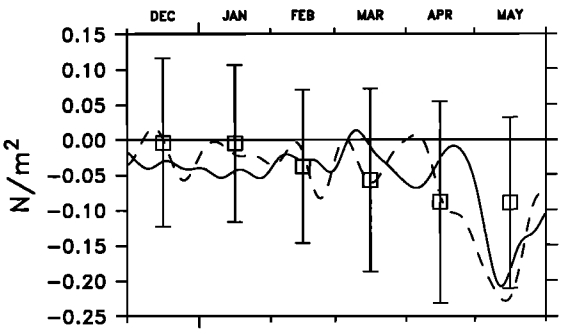

Figure 17. Along-shelf (317°T) wind stress component for the months of December through May. The monthly climatological winds from *Nelson* [1977] are indicated by the squares. As an indication of the variability in observations used by Nelson, approximate standard deviations were found by taking the square root of the sum of the squares of standard deviations for east and north wind stress components (calculated from standard error and observation numbers presented by *Nelson* [1977]). The 1988–1989 30-day low-pass-filtered winds are indicated by the solid line, and the 1981–1982 30-day low-pass-filtered winds by the dashed line.

filtered along-shelf (in the 317°T reference frame) component of wind stress observed from December through May during CODE and SMILE at National Data Buoy Center 46013 (NDBC) 13 and the monthly mean climatological wind stress calculated by *Nelson* [1977] at a 1° square centered at 38°N, 123°W, shows year to year variability in winter and spring wind fields near the SMILE and CODE locations. From December through February, climatological monthly mean winds are near zero but equatorward. Winds during this time in 1988–1989 are equatorward (within approximately 1 standard deviation) of this climatological mean, and winds during 1981–1982 are also equatorward within a standard deviation of the climatological mean. C. E. Dorman et al. (submitted manuscript, 1994) found that the number of equatorward, poleward, and weak wind events during winter of 1988–1989 was fairly typical based on an examination of 10 years of wind records at NDBC 13. Monthly mean winds during spring, prior to the spring transition to upwelling season, are probably also generally equatorward and weak as in Figure 17. All this indicates that a weak mean upwelling may generally be present near 39°N in winter and spring, suggesting a resulting mean offshore heat flux.

The net air-sea heat flux was not a dominant factor in the winter mean heat balance but became so in the spring heat balance. The separation into winter and spring in 1988–1989 is dependent on the mean winter air-sea heat flux being small and on a relatively rapid change to mean spring surface heating prior to the transition to upwelling. Figure 18 shows the 30-day low-passed air-sea heat flux at C3 in 1988–1989 with the climatological heat flux at a 1° square centered at 38°N, 123°W from *Nelson and Husby* [1983]. This shows monthly mean air-sea heat fluxes are indeed small relative to summer values, and may be negative during winter months, and that they increase rapidly in March and April. The spring transition in 1988–1989 occurred in early May 1989, which allowed for 2 months of surface heating prior to the spring transition to upwelling. However, the spring transition is generally thought to occur earlier, in March or April [*Strub and James*, 1988]. This would cut short the spring period of surface heating prior to strong upwelling, so 1988–1989 may be anomalous in this respect. Figure 17 shows the 1988–1989 wind stress plotted with that in 1982 when the spring transition occurred in mid-April [*Lentz*, 1987a].

Another factor which may influence the heat balance is the along-shelf velocity. Through bottom boundary layer dynamics, this may affect the near-bottom cross-shelf heat flux as well as the along-shelf heat flux divergence. Year to year variability is evident in a comparison of 1988–1989 SMILE mean along-shelf currents with those during a similar time of year in 1981–1982 at the same location (see Figure 4 and *Lentz and Chapman* [1989]). However, mean interior along-shelf currents are poleward in both years. If poleward interior currents are a regular part of the seasonal cycle, as *Strub et al.* [1987a] find, they would set up a mean offshore Ekman flow in the bottom boundary layer. The near-bottom onshore heat flux associated with this Ekman flow could be a persistent feature in winter and spring.

Along-shelf velocity is also important in determining the along-shelf temperature gradient flux. It is important to note that the along-shelf temperature gradient flux observed in winter and spring 1988–1989 and winter 1981–1982 was not the result of a mean advection of a mean temperature gradient, but rather was an eddy flux. The physical mechanisms behind the along-shelf temperature gradient flux deserve further study. In winter and spring it is not significantly correlated to the local along-shelf wind, but appears to be associated with mesoscale features. Winter 1981–1982 results at CODE C3 and R3 suggest that the contribution of this term to the heat balance may vary over along-shelf separation scales of 30 km. In summer, *Lentz* [1987b] found an along-shelf heat flux divergence of approximately the same magnitude on the northern California shelf; however, the mean summer along-shelf heat flux divergence was primarily the result of the mean along-shelf advection of a mean temperature field, rather than an eddy heat flux divergence. Fluctuations in the summer along-shelf heat flux divergence were attributed to wind-related occurrences such as relaxation from upwelling [*Send et al.*, 1987] as well as an offshore mesoscale feature. Because the along-shelf temperature gradient flux seems to be associated with mesoscale features and because only a few along-shelf temperature

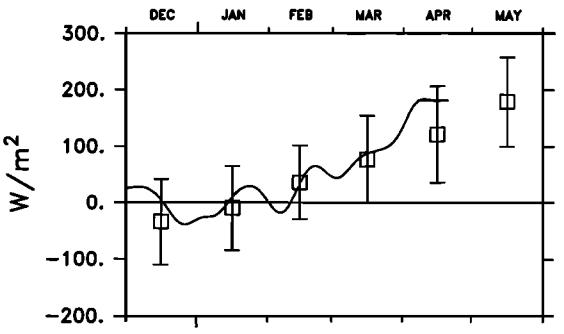

Figure 18. Net surface heat flux for the months of December through May. The monthly climatological air-sea heat flux from *Nelson and Husby* [1983] is indicated by the squares with standard deviations calculated from standard errors and observation numbers presented by *Nelson and Husby* [1983]. The 1988–1989 30-day low-pass-filtered surface heat flux is indicated by the solid line.

gradient fluxes were observed during this study, their effects on a climatological winter heat budget are uncertain.

Appendix A: Estimation of the Net Sea Surface Heat Flux

The net surface heat flux was estimated at C3 as

$$Q = Q_i + Q_b + Q_l + Q_s \quad (10)$$

where Q_i is the net solar radiation, Q_b is the net longwave radiation, Q_l is the latent heat flux, and Q_s is the sensible heat flux. These four terms were estimated using formulas very similar to those employed by *Lentz* [1987b]. The explanation below is taken from that paper with modifications as necessary: $Q_i = I(1 - Ab)$ where I is the measured insolation and Ab is the ocean albedo given by *Payne* [1972]. The insolation was measured at C3 using two types of Eppley pyranometers, a model 8-48 and a model PSP. Because the 8-48 returned a nearly complete record (the PSP failed in early February), we used this instrument for our estimate of net surface heat flux. However, a comparison of the 8-48 data with other available insolation data at C3 and on the coast showed the 8-48 suffered a gain problem, consistently reading low by about 20%. To account for this, we regressed the 8-48 on available C3 PSP data and used this regression coefficient to obtain a more accurate estimate of insolation. $Q_b = Q_{cs} - R$, where the Efimova formula of *Simpson and Paulson* [1979] was used to compute the clear sky upward longwave radiation, Q_{cs}, from the water temperature at 5.5 m, and R is the downward measured longwave radiation reflected from the atmosphere. $Q_s = \rho_a C_P C_h u_w (T_a - T_s)$, where ρ_a is the density of air, C_P is the heat capacity of air, C_h is the sensible heat flux coefficient given by *Friehe and Schmitt* [1976], u_w is the wind speed, T_a is the air temperature 52 km south of C3 at NDBC 13, and T_s is the water temperature at 5.5 m. $Q_l = LC_e u_w (q - q_s)$, where L is the heat of evaporation, C_e is the latent heat flux coefficient given by *Friehe and Schmitt* [1976], q is the absolute humidity given by multiplying the measured relative humidity by the saturation humidity at T_a, and q_s is the absolute humidity at the ocean surface taken to be $0.98 q_{sat}$ at the temperature T_s, where q_{sat} is the saturation humidity. The necessity of using the air temperature at NDBC 13 and the water temperature at 5.5 m causes some uncertainty in longwave, latent, and sensible heat flux estimates. The air temperature at NDBC 13 was used because air temperature records at C3 were lost because of a leak in the vector-averaging wind recorder (VAWR). Comparisons of NDBC 13 to NDBC 14 (located 76 km north of C3) air temperature observations suggest the temperature difference is at most 3°C over 127 km, the distance between NDBC 13 and 14, so that C3 air temperatures are approximately those at NDBC 13. The water temperature at 5.5 m was used because water temperature records at 1 m below the surface were lost owing to leakage in the VAWR at C3.

The net surface heat flux at C3 was assumed to be uniform from C3 to the coast. From shore measurements and the C2 buoy (present in spring) some components of the net sea surface heat flux can be checked for cross-shelf variation. All meteorological variables measured at C3 were also measured on the coast at the Stewart's Point Beach location shown in Figure 1. Stewart's Point and C3 data presented by *Alessi et al.* [1991] show that averages of relative humidity and incoming longwave radiation were within 5% and their standard deviations were within 15%. Wind speed averages and standard deviation do decrease by about a factor of 2 between C3 and the coast. Spring measurements of wind speed at C2 indicate that most of this decrease occurs between C2 and the coast. Neglecting the cross-shelf variation in wind speed probably resulted in an overestimate of the cross-shelf integrated latent heat flux and sensible heat flux. However, sensible and latent heat fluxes were not the largest components of the mean winter and spring net air-sea heat fluxes. These were the mean incoming shortwave radiation and outgoing longwave radiation.

Appendix B: The Winter Heat Budget in 1981–1982

For comparison with the 1988–1989 results the heat balance from 1300 UT on December 12, 1981, to 1200 UT on March 22, 1982, is examined using two moorings deployed on the northern California shelf as part of the Coastal Ocean Dynamics Experiment (CODE). One mooring, denoted CODE C3, was 6 km southeast of the SMILE C3 location. The second mooring was 34 km southeast of the CODE C3 location and was denoted R3. Both moorings were in 90 m of water and had temperature and (VACM) velocity sensors at 9, 35, 55, and 75 m. The C3 mooring had an additional VACM sensor at 15 m. Wind stress data were also acquired at NDBC 13 (located 43 km from C3 and 16 km from R3). The winter CODE data are presented and analyzed by *Lentz and Chapman* [1989]. Though the vertical resolution of the winter CODE data is poorer than that of the SMILE data and the air-sea heat flux cannot be estimated, the winter CODE data appear to be sufficient to resolve the simple vertical structures found in the winter SMILE heat balance (Figure 7). Additionally, historical data [*Nelson and Husby*, 1983] and the winter SMILE results suggest that the surface heat flux is negligible during winter.

The heat budgets at CODE C3 and R3 were estimated using essentially the same methods presented in section 3 except for the along-shelf temperature gradient flux. Because only two moorings were present, the along-shelf temperature gradient at both C3 and R3 was represented by the temperature difference divided by the along-shelf distance between C3 and R3; hence differences in the along-shelf temperature gradient flux between C3 and R3 were entirely due to spatial variations in v. The CODE reference frames [*Winant et al.*, 1987] of 317°T and 329°T at C3 and R3, respectively, were used. Rotation to the reference frame required to make the mean cross-shelf transport at C3 zero (325°T) affected mean heat flux results by only about 10%. The actual local isobath orientation at R3 is not clear, and rotation to other plausible reference frames showed that mean cross-shelf heat flux values at R3 varied from 50% to 200% of the values in the 329°T coordinate frame, though the fluctuating balance was less sensitive.

Both mean and fluctuating heat balances at C3 for 1981–1982 are qualitatively similar to those in 1988–1989 both in the magnitude of the vertically integrated budget (Table B1) and in vertical structure. The mean offshore heat flux in the upper 30 m is approximately balanced by mean cooling and an eddy along-shelf temperature gradient flux. The low-passed fluctuating heat balance in 1981–1982 is again an

Table B1. Estimated Terms in Winter 1981–1982 Heat Balances at C3 and R3

	Mean	Eddy Contribution to Mean	Standard Error	Standard Deviation
Heat content change at C3*	−4.1	...	6.7	52.3
Cross-shelf heat flux at C3*	−15.5	−3.8	6.5	50.3
Along-shelf temperature gradient flux at C3†	7.0	7.3	3.1	19.9
Heat balance residual at C3†	−4.4	...	7.7	49.0
Heat content change at R3*	−6.0	...	10.2	78.8
Cross-shelf heat flux at R3*	−8.5	−1.4	7.8	60.2
Along-shelf temperature gradient flux at R3†	−3.6	−3.2	4.0	25.0
Heat balance residual at R3†	−6.9	...	10.1	63.6

Heat budget units are in 10^5 W m^{-1}. Standard error estimates are calculated as in Table 1.
*Standard error assumes integral timescale of 40 hours.
†Standard error assumes integral timescale of 60 hours.

Table B2. Low-Passed Correlation Coefficients for Winter 1981–1982 Balances at C3 and R3

		C3			R3		
	Along-Shelf Wind Stress	Heat Content	Cross-Shelf Heat Flux	Along-Shelf Temperature Gradient Flux	Heat Content	Cross-Shelf Heat Flux	Along-Shelf Temperature Gradient Flux
Along-shelf wind stress	1	0.73	0.54	0.25	0.70	0.67	0.08
C3 heat content		1	0.56	0.33	0.57	0.52	0.17
C3 cross-shelf heat flux			1	0.19	0.38	0.38	0.24
C3 along-shelf temperature gradient flux				1	0.27	0.07	0.52
R3 heat content					1	0.65	0.10
R3 cross-shelf heat flux						1	0.04
R3 along-shelf temperature gradient flux							1

Integral timescales are as in Table 3. Correlations of 0.17, 0.25, and 0.33 are significant at the 80%, 95%, and 99% levels, respectively, for wind stress, heat content change, and cross-shelf heat flux. Correlations of 0.20, 0.30, and 0.39 involving along-shelf temperature gradient flux are significant at the 80%, 95%, and 99% levels, respectively.

approximate balance, (9), between changes in heat content and cross-shelf heat flux which are well correlated (Table B2) with the wind stress. The along-shelf temperature gradient flux is uncorrelated with the wind and becomes important only during several events. Though the 1981–1982 heat balance at C3 is similar to that in 1988–1989, spatial differences between C3 and R3 did exist. The offshore heat flux at C3 is larger than that at R3, and the mean along-shelf temperature gradient flux, which adds at C3, removes it at R3. These qualitative results are not sensitive to changes in the R3 coordinate frame.

Acknowledgments. Financial support was provided by NSF grant OCE 91-15713. We thank all who contributed to the SMILE field program, especially Russ Davis and Lloyd Regier at Scripps Institution of Oceanography and Rick Trask, George Tupper, Paul Bouchard, Joe Poirier, Jerry Dean, Dave Simoneau, and Bob Beardsley at WHOI. Special thanks are also extended to Brad Butman at USGS Woods Hole for making available his subsurface mooring data. Susan Tarbell's and Carol Alessi's efforts in processing the SMILE time series are appreciated, as are the efforts of Dick Limeburner in acquiring and processing the SMILE CTD data. We also thank Bob Beardsley, Ken Brink, and two anonymous reviewers for their critiques of this manuscript and Clive Dorman, Amelito Enriquez, and Carl Friehe for helpful discussions. WHOI contribution 8477.

References

Alessi, C. A., S. J. Lentz, and R. C. Beardsley, The Shelf Mixed Layer Experiment (SMILE): Program overview and moored and coastal array data report, *WHOI Tech. Rep. 91-39*, 211 pp., Woods Hole Oceanogr. Inst., Woods Hole, Mass., 1991.

Beardsley, R. C., and S. J. Lentz, The Coastal Ocean Dynamics Experiment collection: An introduction, *J. Geophys. Res.*, *92*, 1455–1464, 1987.

Bryden, H. L., D. Halpern, and R. D. Pillsbury, Importance of eddy heat flux in a heat budget for Oregon coastal waters, *J. Geophys. Res.*, *85*, 6649–6653, 1980.

Friehe, C. A., and K. F. Schmitt, Parameterization of air-sea heat fluxes of sensible heat and moisture by bulk aerodynamical formulas, *J. Phys. Oceanogr.*, *6*, 801–809, 1976.

Gross, T. F., A. E. Isley, and C. R. Sherwood, Estimation of stress and bed roughness during storms on the northern California shelf, *Cont. Shelf Res.*, *12*, 389–413, 1992.

Halliwell, G. R., and J. S. Allen, The large-scale wind field along the west coast of North America, 1981–1982, *J. Geophys. Res.*, *92*, 1861–1884, 1987.

Hickey, B. M., and N. E. Pola, The seasonal alongshore pressure gradient on the west coast of the United States, *J. Geophys. Res.*, *88*, 7623–7633, 1983.

Huyer, A., Hydrographic observations along the CODE central line off northern California, 1981, *J. Phys. Oceanogr.*, *14*, 1647–1658, 1984.

Largier, J. L., B. A. Magnell, and C. D. Winant, Subtidal circulation

over the northern California shelf, *J. Geophys. Res.*, *98*, 18,147–18,179, 1993.

Lentz, S. J., A description of the 1981 and 1982 spring transitions over the northern California shelf, *J. Geophys. Res.*, *92*, 1545–1567, 1987a.

Lentz, S. J., A heat budget for the northern California shelf during CODE 2, *J. Geophys. Res.*, *92*, 14,491–14,509, 1987b.

Lentz, S. J., The surface boundary layer in coastal upwelling regions, *J. Phys. Oceanogr.*, *22*, 1517–1539, 1992.

Lentz, S. J., and D. C. Chapman, Seasonal differences in the current and temperature variability over the northern California shelf during the Coastal Ocean Dynamics Experiment, *J. Geophys. Res.*, *94*, 12,571–12,592, 1989.

Limeburner, R. (Ed.), CODE-2: Moored array and large-scale data report, *WHOI Tech. Rep. 85-35*, 234 pp., Woods Hole Oceanogr. Inst., Woods Hole, Mass., 1985.

Limeburner, R., and R. C. Beardsley, CTD observations off northern California during the Shelf Mixed Layer Experiment, SMILE, November 1988, *WHOI Tech. Rep. 91-25*, 272 pp., Woods Hole Oceanogr. Inst., Woods Hole, Mass., 1989a.

Limeburner, R., and R. C. Beardsley, CTD observations off northern California during the Shelf Mixed Layer Experiment, SMILE, February/March 1989, *WHOI Tech. Rep. 91-41*, 218 pp., Woods Hole Oceanogr. Inst., Woods Hole, Mass., 1989b.

Limeburner, R., and R. C. Beardsley, CTD observations off northern California during the Shelf Mixed Layer Experiment, SMILE, May 1989, *WHOI Tech. Rep. 91-42*, 239 pp., Woods Hole Oceanogr. Inst., Woods Hole, Mass., 1989c.

Nelson, C. S., Wind stress and wind stress curl over the California Current, *NOAA Tech. Rep. NMFS SSRF*, *714*, 87 pp., 1977.

Nelson, C. S., and D. M. Husby, Climatology of surface heat fluxes over the California Current region, *NOAA Tech. Rep. NMFS SSRF*, *763*, 155 pp., 1983.

Payne, R. E., Albedo of the sea surface, *J. Atmos. Sci.*, *29*, 959–970, 1972.

Richman, J. G., and A. Badan-Dangon, Mean heat and momentum budgets during upwelling for the coastal waters off northwest Africa, *J. Geophys. Res.*, *88*, 2626–2632, 1983.

Rudnick, D. L., and R. E. Davis, Mass and heat budgets on the northern California shelf, *J. Geophys. Res.*, *93*, 14,013–14,024, 1988.

Santala, M. J., Surface-referenced current meter measurements, Ph.D. thesis, Mass. Inst. of Technol./Woods Hole Oceanogr. Inst., Woods Hole, Mass., 1991.

Send, U., The origin of eddy heat fluxes in the northern California upwelling regime, *J. Geophys. Res.*, *94*, 871–876, 1989.

Send, U., R. C. Beardsley, and C. D. Winant, Relaxation from upwelling in the Coastal Ocean Dynamics Experiment, *J. Geophys. Res.*, *92*, 1683–1698, 1987.

Simpson, J. J., and C. A. Paulson, Mid-ocean observations of atmospheric radiation, *Q. J. R. Meteorol. Soc.*, *105*, 487–502, 1979.

Strub, P. T., and C. James, Atmospheric conditions during the spring and fall transitions in the coastal ocean off western United States, *J. Geophys. Res.*, *93*, 15,561–15,584, 1988.

Strub, P. T., J. S. Allen, A. Huyer, R. L. Smith, and R. C. Beardsley, Seasonal cycles of currents, temperatures, winds, and sea level over the northeast Pacific continental shelf: 35°N to 48°N, *J. Geophys. Res.*, *92*, 1507–1526, 1987a.

Strub, P. T., J. S. Allen, A. Huyer, and R. L. Smith, Large-scale structure of the spring transition in the coastal ocean off North America, *J. Geophys. Res.*, *92*, 1527–1544, 1987b.

Trowbridge, J. H., and S. J. Lentz, Asymmetric behavior of an oceanic boundary layer above a sloping bottom, *J. Phys. Oceanogr.*, *21*, 1171–1185, 1991.

Weatherly, G. L., and P. L. Martin, On the structure and dynamics of the oceanic bottom boundary layer, *J. Phys. Oceanogr.*, *8*, 557–570, 1978.

Winant, C. D., R. C. Beardsley, and R. E. Davis, Moored wind, temperature, and current observations made during Coastal Ocean Dynamics Experiments 1 and 2 over the northern California shelf and upper slope, *J. Geophys. Res.*, *92*, 1569–1604, 1987.

E. P. Dever and S. J. Lentz, Department of Physical Oceanography, Woods Hole Oceanographic Institution, Woods Hole, MA 02543.

(Received September 2, 1993; revised May 6, 1994;
accepted May 9, 1994.)